Struct Chem (2015) 26:301–318
DOI 10.1007/s11224-014-0485-4

ORIGINAL RESEARCH

# Theoretical investigation of the N → Sn coordination in $(Me_3SnCN)_2$

**Piotr Matczak**

Received: 15 July 2014 / Accepted: 25 July 2014 / Published online: 20 August 2014


**Abstract** The N → Sn coordination occurring in the $(Me_3SnCN)_2$ dimer has been investigated using various computational methods and several theoretical tools possessing great interpretative potential. The dimer is formed by moving the C≡N fragment of the first $Me_3SnCN$ molecule close to the Sn atom of the second molecule and the resulting N → Sn coordination corresponds to that observed in the crystal structure of trimethyltin cyanide. The geometry of $(Me_3SnCN)_2$ is optimized using the MP2 method and its 11 variants, and then it is compared with the reference geometry obtained at the CCSD level of theory. SCS-MP2 reproduces best the reference geometry of $(Me_3SnCN)_2$ and its accuracy is close to that of the MP4 (SDQ) method. Two families of basis sets, namely the correlation-consistent basis sets proposed by Dunning and co-workers and the 'def2' basis sets developed by Ahlrichs and co-workers, are taken into account and their effect on the geometry of the dimer is examined in detail. The intermolecular interaction in $(Me_3SnCN)_2$ has been analyzed using SAPT, NBO, QTAIM, and ELF. The results indicate that the $(Me_3SnCN)_2$ dimer possesses a weak N → Sn coordination bond whose character is predominantly ionic. A value of −7.64 kcal/mol is proposed to be the best estimate of the interaction energy between the $Me_3SnCN$ molecules in the dimer.

**Keywords** Organotin(IV) compounds · Trimethyltin cyanide · N → Sn coordination · Ab initio methods

## Introduction

Organotin(IV) compounds (in other words, organostannanes) attracted great attention in the past decades because of their industrial and agricultural significance [1, 2]. The stabilization of poly(vinyl chloride) plastics seems to be their principal industrial application, while their fungicidal, bactericidal, and insecticidal activity turned out to be useful for agriculture. Although the biological activity of these compounds was desirable for many applications, some issues associated with their harmful impact on the environment were also raised [3, 4]. More recently, the possibility of using some organotin(IV) compounds in medicine has become the focus of extensive exploration [5, 6]. In the area of academic research, organotin(IV) compounds are considered to be reagents valuable for laboratory organic synthesis, e.g., in various reduction, transmetallation, and coupling reactions [1, 7]. Aside from such synthetic applications, an interesting aspect of organotin(IV) compounds is their structural diversity. Organotin(IV) compounds often form structures in which previously tetravalent Sn atoms exhibit the coordination number greater than four, that is, the Sn atoms become hypervalent [1, 8, 9]. In such cases, the Sn atoms are involved in additional inter- and/or intramolecular interactions that expand their coordination number and, consequently, change their tetrahedral configuration. The appearance of such additional interactions results from the pronounced electron-acceptor ability of the Sn atoms and, in the presence of electron donors D, it leads to the

**Electronic supplementary material** The online version of this article (doi:10.1007/s11224-014-0485-4) contains supplementary material, which is available to authorized users.

P. Matczak (✉)
Department of Theoretical and Structural Chemistry, University of Łódź, Pomorska 163/165, 90-236 Lodz, Poland
e-mail: p.a.matczak@gmail.com

formation of dative D → Sn bonds (also known as coordination bonds). Nitrogen, oxygen, and halogen atoms are most often the electron donors as they can easily provide a lone electron pair to the Sn atom [9].

The structural implications of an increase in the Sn-atom coordination number caused by the intermolecular N → Sn coordination were determined experimentally for the first time for trimethyltin chloride in the early 1960s [10, 11]. The N atom of pyridine was involved in the formation of the N → Sn bond with $Me_3SnCl$ and the resulting structure was trigonal bipyramidal. In general, the change in coordination number from four to five is frequently observed for organotin(IV) molecules, especially for those containing four Sn–C bonds [8]. Then, the formation of the intermolecular N → Sn bond leads to the pentacoordinated Sn atom that usually adopts an approximately trigonal bipyramidal coordination geometry. The electron-acceptor ability of the Sn atom can be strengthened by the presence of one or more electronegative groups bonded to the Sn atom. In the trigonal bipyramidal configuration of the pentacoordinated Sn atom, the most electronegative groups normally occupy the axial positions and the bonds between those groups and the Sn atom are longer than the bonds between Sn and groups in the equatorial positions. If an organotin(IV) molecule contains a group with an N atom possessing the lone electron pair, then the N atom can act as the electron donor for the N → Sn bond with another organotin(IV) molecule of the same type. It allows a large number of organotin(IV) molecules to form the N → Sn bonds between each other and, in consequence, a coordination polymer may be obtained. Trimethyltin cyanide is a good example of the organotin(IV) compound, whose crystal structure exhibits a polymeric association with the intermolecular N → Sn bonding motif. The molecules of $Me_3SnCN$ are arranged in linear chains with tin atoms pentacoordinated in an approximately trigonal bipyramidal configuration. Each tin atom is surrounded by three Me groups in the equatorial positions and two CN fragments in the axial positions. The chains of $Me_3SnCN$ molecules with an ordered C–N–Sn–C–N environment run parallel to each other and these form the structure of crystalline trimethyltin cyanide [12].

In the present work, the results of a theoretical investigation performed for the trimethyltin cyanide dimer $(Me_3SnCN)_2$ are reported. The Sn–C≡N axes of both $Me_3SnCN$ molecules in this dimer were arranged along a single line and the cyano group of the first $Me_3SnCN$ molecule was adjacent to the Sn atom of the second $Me_3SnCN$ molecule. Therefore, this dimer could be considered to be an appropriate model system for the computational investigation of the intermolecular N → Sn coordination. On the one hand, the dimer was small enough to employ a relatively broad range of theoretical methods, but, on the other hand, it was not oversimplified because such a dimer demonstrates the intermolecular N → Sn coordination present in the chains of $Me_3SnCN$ molecules that constitute the structure of crystalline trimethyltin cyanide [12].

This work has two main goals. The first one is to select an appropriate wave function-based theory (WFT) methodology for the investigations of the intermolecular N → Sn coordination as it will be exemplified by $(Me_3SnCN)_2$. The overwhelming majority of current theoretical studies devoted to organotin(IV) compounds whose structures exhibit hypervalent Sn atoms [13–15] have been carried out using various density functional theory (DFT) methods [16]. The enormous popularity of DFT methods stems from the fact that these methods are capable of including a large fraction of electron correlation at an affordable computational cost and thus they are considered as the natural theory for systems with a large number of electrons and with strong electron correlation effects. In consequence, DFT methods have been widely used for modeling organometallic molecules and inorganic complexes of both transition metals [17–19] and main group metals [20–22]. Before the advent of DFT methods, molecules and complexes containing metal atoms were usually investigated using the second-order Møller–Plesset perturbation theory (MP2) [23, 24], which is the simplest and most economical post-Hartree–Fock WFT method. Unfortunately, the MP2 method was not able to provide the accurate description of many systems with metal atoms [25], especially those with *3d* transition metals [26]. Compared to DFT, the MP2 method turned out to be computationally more demanding. As a result of these drawbacks, the MP2 method lost some of its appeal for the investigations of systems with metal atoms. In the last years there were, however, many attempts to improve the accuracy of the MP2 method [27–38] and to decrease its computational cost [39–41]. Among the most important improvements in the accuracy of MP2, one can mention various spin-component scaling (SCS) schemes [27–34] and the orbital-optimized (OO) approach [36], whereas the application of the resolution of the identity (RI) technique [39] leads to dramatic speedups of MP2 calculations. As the first goal of the present work, we would like to establish whether such recently proposed modifications allow the MP2 method to achieve higher accuracy in predicting the structural and energetic parameters that describe the $(Me_3SnCN)_2$ dimer. This dimer is a closed-shell system containing the main group metal and, therefore, we expect that some variants of the MP2 method may turn out to be an attractive alternative to DFT for such kind of systems. Some effects associated with combining the MP2 method and its variants with different basis sets will be also taken into consideration.

So far the intermolecular N → Sn coordination in trimethyltin cyanide has been investigated theoretically only in the context of its $^{119}$Sn NMR properties [12, 42]. Moreover, the theoretical studies of the intermolecular N → Sn coordination in other organotin(IV) compounds are generally rare [43–45]. Therefore, the second goal of the present work is to provide insight into the intermolecular N → Sn coordination in the $(Me_3SnCN)_2$ dimer. Several theoretical tools will be employed to describe the interaction between the $Me_3SnCN$ molecules in this dimer and, in consequence, to characterize the N → Sn bond.

## Theoretical methods

The geometry of the $(Me_3SnCN)_2$ dimer was optimized by the MP2 method in both its conventional form and its 11 variants. It is known that the MP2 method in its conventional form leads to an overbinding for the systems in which significant dispersion forces occur [27]. The reason lying behind this overbinding is the uncoupled Hartree–Fock treatment of dispersion in the MP2 method. One of the possibilities for improving the accuracy of the MP2 method is to use a SCS scheme [27]. Such a scheme is based on a partitioning of the MP2 electron correlation energy into contributions from antiparallel- (or opposite-) and parallel-spin (or same-spin) pairs of electrons. Separate scaling coefficients (usually denoted by $c_{os}$ and $c_{ss}$) are applied to these two contributions. The scaling coefficients can be either deduced from theory or parametrized against some benchmark data. The SCS-MP2 variant makes use of the original SCS scheme ($c_{os} = 1.20$ and $c_{ss} = 0.33$) proposed by Grimme [27] but many modifications of the original scheme were also proposed [28, 30–34]. Aside from SCS-MP2, other four variants that can be expressed by the respective SCS schemes, namely SOS-MP2 [28], FE2-MP2 [30], SCS(MI)-MP2 [31], and S2-MP [34], were adopted in the present work. These four variants differ in the values of the $c_{os}$ and $c_{ss}$ coefficients from the original SCS scheme. Additionally, the conventional MP2 method and the above-mentioned variants were also combined with the OO approach. In this approach, the orbital optimization is achieved by the minimization of Hylleraas functional with respect to both double excitation amplitude variations and orbital rotations. Although the OO approach allows the MP2 method to improve its accuracy for some systems, e.g., those suffering from the imbalance in the Hartree–Fock treatment of the Coulomb and exchange holes, the computational cost of the OO-MP2 variant is substantially higher than that of MP2. In order to enhance the computational efficiency of both the conventional MP2 method and its all variants, our calculations of expensive electron repulsion integrals were reduced by the RI technique. The utilization of this technique leads to computational savings amounting to ca. 1 order of magnitude compared to the computational cost of corresponding non-RI calculations. Errors introduced by the RI technique are minor and tend to cancel each other when chemically relevant energy differences are calculated. TURBOMOLE 6.3.1 [46] and ORCA 3.0.1 [47] were used to carry out the non-OO and OO calculations, respectively. The same tight convergence criteria for the optimization procedure were imposed in both programs.

The $(Me_3SnCN)_2$ geometry optimized by the MP2 method and its variants was compared with the reference geometry obtained at the CCSD level of theory [48]. The experimental geometry of $(Me_3SnCN)_2$ in the gas phase is not known and the application of such advanced WFT methods as QCISD(T) or CCSD(T) for the geometry optimization of this dimer was beyond the capabilities of our computer system. The CCSD method turned out to be the highest level of theory that could be employed in the optimization of the dimer. The CCSD method was previously used for obtaining reference geometries of molecular complexes [49, 50] but it is known that the performance of this method may be worse for the geometries of single molecules [51]. The dimer was additionally optimized using the MP4(SDQ) method [24, 52] and this method was selected rather to provide the $(Me_3SnCN)_2$ geometry estimating the limit reached within the Møller–Plesset perturbation theory than to determine the true geometry of $(Me_3SnCN)_2$. The CCSD and MP4(SDQ) optimizations were performed using GAUSSIAN 09 D.01 [53]. Analytic gradients were used for both CCSD and MP4(SDQ) in this program, which significantly speeded up the geometry optimization of $(Me_3SnCN)_2$. Unfortunately, the RI technique is not available in the program. The comparison of the $(Me_3SnCN)_2$ structures optimized by different methods was made using the minimized root-mean-square value of the residual distances between the corresponding atoms belonging to these structures. This quantity is denoted here as RMSD and its values were computed with HYPERCHEM 8.0 [54].

The results presented in this work were obtained using essentially two families of basis sets. The correlation-consistent basis sets proposed by Dunning [55], (aug)-cc-pV*X*Z, belonged to the first family. For the Sn atoms, these basis sets were employed in the (aug)-cc-pV*X*Z-PP version developed by Peterson [56], which means that Stuttgart-Koeln MCDHF RSC pseudopotential [57] replacing 28 core electrons was assigned to the Sn atoms. We took into account the cardinal number $X$ ranging from D to 5. The second family of the basis sets considered in this work was composed of Ahlrichs' basis sets in their 'def2' version developed by Weigend [58]. The def2-SVP, def2-TZVPP, and def2-QZVPP basis sets were also augmented with

diffuse functions [59]. Similarly to the (aug)-cc-pV*X*Z-PP basis sets, the 'def2' ones made use of a pseudopotential that described 28 core electrons in each Sn atom. However, the pseudopotential present in the 'def2' basis sets is a slightly modified version of the pseudopotential incorporated into (aug)-cc-pV*X*Z-PP.

The interaction energy $E_{int}$ between the $Me_3SnCN$ molecules in the $(Me_3SnCN)_2$ dimer was calculated mostly in the supermolecular fashion. The sum of the total energies of both $Me_3SnCN$ molecules in their geometries found in $(Me_3SnCN)_2$ was subtracted from the total energy of the dimer. In order to remove the basis-set superposition error (BSSE) from the $E_{int}$ values, the counterpoise correction proposed by Boys and Bernardi [60] was employed. The $E_{int}$ values were also extrapolated to the complete basis set (CBS) limit using the procedure of Halkier et al. [61, 62] (details of the extrapolation procedure can be found in Section S2, Electronic supplementary material).

The intermolecular N → Sn coordination in $(Me_3SnCN)_2$ was analyzed using symmetry-adapted perturbation theory (SAPT) [63, 64], natural bond orbital (NBO) analysis [65], the quantum theory of atoms in molecules (QTAIM) [66], and electron localization function (ELF) [67]. The SAPT decomposition of the interaction between the $Me_3SnCN$ molecules in the dimer was performed with SAPT2012.2 [68] (more details of the SAPT calculation can be found in Section S3, Electronic supplementary material). The NBO code [69] attached to TURBOMOLE and GAUSSIAN allowed us to do the NBO analysis. MULTIWFN 3.2.1 [70] was used to conduct the QTAIM and ELF analyses.

## Results and discussion

We start with establishing how accurately the $(Me_3SnCN)_2$ geometries obtained by the MP2 method and its variants reproduce the geometry optimized at the CCSD level of theory. In order to provide a comprehensive indicator of the accuracy of MP2 and its variants, the RMSD between the atoms belonging to the $(Me_3SnCN)_2$ structure optimized using each of the MP2-based methods and the corresponding atoms of the dimer optimized by CCSD was calculated. The resulting values of RMSD are presented graphically in Fig. 1 (the numerical values of RMSD are listed in Table S2, Electronic supplementary material). The values of RMSD express quantitatively the deviation of the geometries optimized by the MP2-based methods from the CCSD geometry. The lower the value of RMSD for a given MP2-based method is obtained, the smaller the difference in the $(Me_3SnCN)_2$ geometries yielded by this MP2-based method and by CCSD occurs. We were able to assess the accuracy of the $(Me_3SnCN)_2$ geometries predicted by the MP2 method and its variants in combination with the double-ζ basis sets. The reason for the application of such basis sets was the very high computational cost of the CCSD method used for obtaining the reference geometry of the dimer. It is clear from what Fig. 1 shows that SCS-MP2 gives the lowest values of RMSD for all four basis sets. The OO-SOS-MP2 variant also performs well when it is combined with cc-pVDZ, def2-SVP, or def2-SVPD. Then, it produces the values of RMSD smaller than 0.01 Å. The RMSD values yielded by SCS-MP2 are more than one order of magnitude smaller than the corresponding values obtained by the variant that constitutes the opposite extreme of RMSD, namely OO-MP2. The SCS-MP2 variant outperforms the conventional MP2 method considerably. The improvement in geometry predicted by SCS-MP2 over that optimized by MP2 was previously reported for various systems containing gold [71, 72] and for some systems with dative metal–metal bonds [73].

It is interesting to examine the convergence of the $(Me_3SnCN)_2$ geometries optimized using the MP2 method and its variants to the geometry calculated at the MP4(SDQ) level of theory. The MP4(SDQ) method seems to be the highest level of Møller–Plesset perturbation theory that can be routinely employed in the optimization of $(Me_3SnCN)_2$ and the MP4(SDQ)-optimized geometry may be a practical estimate of the limit of accuracy for Møller–Plesset perturbation theory. Our discussion will focus on one intermolecular distance and the RMSD between the atoms of $(Me_3SnCN)_2$ optimized using each of the MP2-based methods and the corresponding atoms of the dimer optimized at the MP4(SDQ) level of theory. The value of $d_{N\rightarrow Sn}$, that is the distance between the N atom of the first $Me_3SnCN$ molecule (denoted as **1**, see Fig. 2) and the Sn atom of the second $Me_3SnCN$ molecule (denoted as **2**), will be examined because $d_{N\rightarrow Sn}$ is a fundamental, geometrical parameter describing the N → Sn coordination in the dimer. The N atom of **1** acts as the Lewis base center, whereas the Sn atom of **2** plays the role of the Lewis acid center. We managed to optimize the dimer using MP4(SDQ) in combination with four basis sets. A pair of Dunning's double-ζ basis sets (one without and another with diffuse functions) and an analogous pair of Ahlrichs' basis sets were used to check whether the convergence of the MP2-based methods is dependent on such basis-set effects as the kind of basis set and the presence of diffuse functions. The values of $d_{N\rightarrow Sn}$ and RMSD in the $(Me_3SnCN)_2$ geometries obtained by MP2 and its 11 variants are shown in Table 1. The SCS-MP2, SOS-MP2, and SCS(MI)-MP2 variants lead to an elongation of the $d_{N\rightarrow Sn}$ distance compared to the value of $d_{N\rightarrow Sn}$ predicted by the MP4(SDQ) method, whereas a compression of $d_{N\rightarrow Sn}$ is observed for the $(Me_3SnCN)_2$ geometries optimized by MP2, FE2-MP2, and S2-MP. The application of

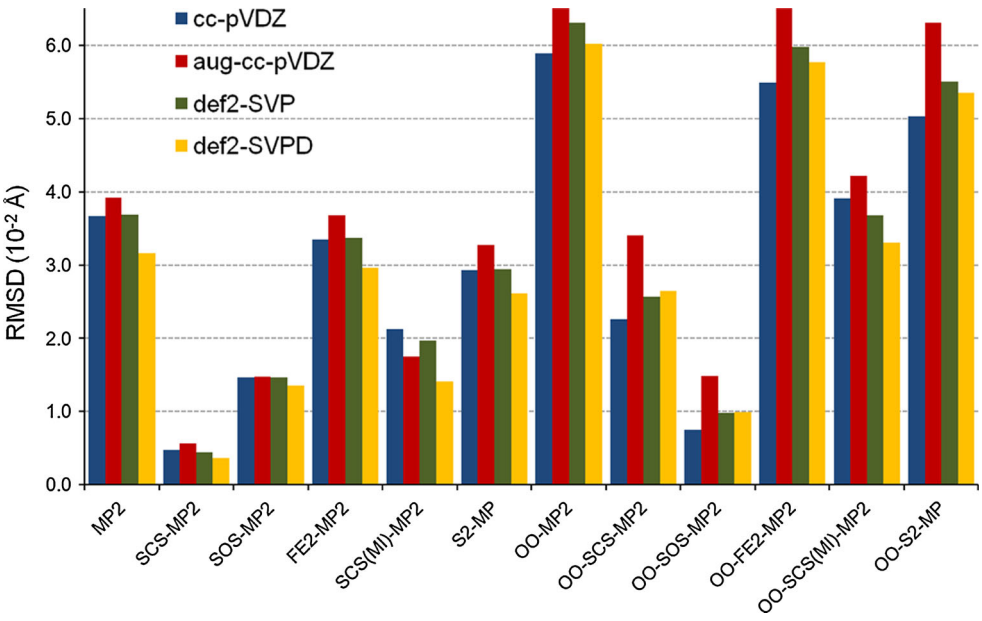


**Fig. 1** RMSD for the $(Me_3SnCN)_2$ geometries obtained by MP2 and its variants in combination with four basis sets (Color figure online)

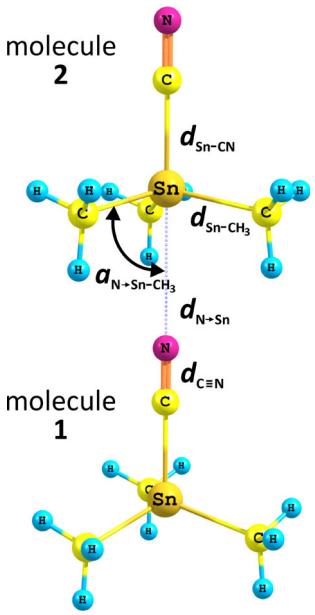


**Fig. 2** Geometry of $(Me_3SnCN)_2$ optimized using SCS-MP2/aug-cc-pVQZ. *Symbols* denoting selected geometrical parameters and numbering of individual $Me_3SnCN$ molecules in the dimer are also shown. The N → Sn bond is represented by a *dotted line* (Color figure online)

the OO approach to the MP2 method and its variants always results in the compression of $d_{N\rightarrow Sn}$. As seen in Table 1, the OO-MP2 method gives the shortest $d_{N\rightarrow Sn}$ distance. Compared to the MP4(SDQ) value of $d_{N\rightarrow Sn}$, the one yielded by OO-MP2 is 0.112-0.146 Å shorter, depending on the basis set used. The analysis of RMSD reveals that the SCS-MP2-optimized geometry is the closest to that optimized at the MP4(SDQ) level of theory. The excellent convergence of the SCS-MP2 geometry toward the MP4(SDQ) one can be observed for both (aug)-cc-pVDZ and def2-SVP(D). The SCS-MP2 method combined with all four basis sets leads to the values of RMSD that do not exceed 0.006 Å. The RMSD values for SCS-MP2 mixed with the diffuse-augmented basis sets are slightly smaller than the values obtained without using diffuse functions. The OO-SOS-MP2 variant also provides good convergence to MP4(SDQ) for the $(Me_3SnCN)_2$ geometry.

Since the SCS-MP2 variant reproduces best the $(Me_3SnCN)_2$ geometry obtained by the CCSD method and, additionally, it is computationally less demanding than the OO-SOS-MP2 variant, it is possible to inspect the $(Me_3SnCN)_2$ geometry optimized by SCS-MP2 in conjunction with much larger basis sets than (aug)-cc-pVDZ and def2-SVP(D). We are interested in determining how the geometry of $(Me_3SnCN)_2$ changes in the sequences of basis sets whose size grows gradually. Selected geometrical parameters characterizing the dimer are marked in Fig. 2 and their values obtained by SCS-MP2 mixed with various basis sets are presented in Table 2. There is a clear trend in the tabulated values of three parameters describing the inner geometries of the $Me_3SnCN$ molecules in the dimer, that is, $d_{C\equiv N}$ and $d_{Sn-CN}$ and $d_{Sn-CH_3}$. In order to distinguish between the C atom of cyano group and the C atom of methyl group, the two types of C atoms will be marked in this work by 'CN' and '$CH_3$,' respectively. The $d_{C\equiv N}$, $d_{Sn-CN}$, and $d_{Sn-CH_3}$ distances get compressed monotonously, while the size of basis sets grows. It is valid for all four sequences of cc-pV*X*Z, aug-cc-pV*X*Z (where $X$ = D, T, Q), def2-*Y*(Z)VP(P), and def2-*Y*(Z)VP(P)D (where $Y$ = S, T, Q). The decreases in the values of the three distances are more significant for the enlargement of

**Table 1** $d_{N\rightarrow Sn}$ and RMSD (in parentheses) for the $(Me_3SnCN)_2$ geometries obtained by MP2 and its variants in combination with four basis sets

| Method | Basis set | | | |
|---|---|---|---|---|
| | cc-pVDZ | aug-cc-pVDZ | def2-SVP | def2-SVPD |
| MP2 | 3.035 (2.863) | 2.889 (3.013) | 3.091 (2.851) | 2.884 (2.594) |
| SCS-MP2 | 3.100 (0.528) | 2.955 (0.515) | 3.159 (0.584) | 2.937 (0.420) |
| SOS-MP2 | 3.135 (2.243) | 2.993 (2.349) | 3.194 (2.273) | 2.965 (1.890) |
| FE2-MP2 | 3.036 (2.530) | 2.888 (2.771) | 3.094 (2.527) | 2.882 (2.397) |
| SCS(MI)-MP2 | 3.107 (1.636) | 2.981 (1.591) | 3.163 (1.432) | 2.967 (1.433) |
| S2-MP | 3.044 (2.121) | 2.896 (2.357) | 3.102 (2.105) | 2.889 (2.040) |
| OO-MP2 | 2.973 (5.065) | 2.809 (6.137) | 3.018 (5.459) | 2.826 (5.449) |
| OO-SCS-MP2 | 3.050 (1.444) | 2.883 (2.491) | 3.100 (1.742) | 2.892 (2.075) |
| OO-SOS-MP2 | 3.090 (0.839) | 2.925 (0.790) | 3.141 (0.804) | 2.927 (0.595) |
| OO-FE2-MP2 | 2.976 (4.665) | 2.809 (5.836) | 3.020 (5.135) | 2.826 (5.193) |
| OO-SCS(MI)-MP2 | 3.057 (3.165) | 2.908 (3.408) | 3.115 (2.897) | 2.908 (2.824) |
| OO-S2-MP | 2.985 (4.212) | 2.818 (5.388) | 3.030 (4.661) | 2.834 (4.776) |
| MP4(SDQ) | 3.098 | 2.954 | 3.157 | 2.938 |

$d_{N\rightarrow Sn}$ values in Å, RMSD values in $10^{-2}$ Å

The values of $d_{N\rightarrow Sn}$ calculated by MP4(SDQ) are also shown

basis sets from double to triple ζ than for the subsequent enlargement from triple to quadruple ζ. The addition of diffuse functions to the largest basis sets, namely cc-pVQZ and def2-QZVPP, practically does not change the values of $d_{C\equiv N}$, $d_{Sn-CN}$, and $d_{Sn-CH_3}$. Thus, the cc-pVQZ and def2-QZVPP basis sets are sufficiently saturated to provide convergent values of parameters characterizing the inner geometries of the $Me_3SnCN$ molecules in the dimer. The $d_{N\rightarrow Sn}$ parameter, which directly describes the N → Sn coordination, exhibits a different basis set dependence. For the sequences of cc-pV*X*Z and aug-cc-pV*X*Z, the basis sets with $X = T$ lead to the greatest values of $d_{N\rightarrow Sn}$. These longest distances between the $Me_3SnCN$ molecules are accompanied by the smallest distortion of the geometry about the Sn atom of **2** from the tetrahedral arrangement (for which $a_{N\rightarrow Sn-CH_3}$ would be equal to 70.5°). Thus, the value of $a_{N\rightarrow Sn-CH_3}$ obtained using the basis set with $X = T$ is the closest to 70.5° in each of the two sequences. The addition of diffuse functions to Dunning's basis sets results in moving the $Me_3SnCN$ molecules closer to each other in the dimer and, therefore, going from cc-pV*X*Z to aug-cc-pV*X*Z increases the $a_{N\rightarrow Sn-CH_3}$ angle for each *X*. In the case of the def2-*Y*(Z)VP(P) basis sets, there is a gradual decrease in the values of $d_{N\rightarrow Sn}$ when the size of these basis sets changes from $Y = S$ to $Y = T$ and then to $Y = Q$. Surprisingly, the opposite trend in the values of $d_{N\rightarrow Sn}$ is observed in the sequence of the def2-*Y*(Z)VP(P)D basis sets. When a pair of def2-*Y*(Z)VP(P) and def2-*Y*(Z)VP(P)D with $Y = S$ or T is considered, the presence of diffuse functions moves two $Me_3SnCN$ molecules closer to one another, and such an effect of diffuse functions is common to Dunning's and Ahlrichs' basis sets. The effect of diffuse functions on $d_{N\rightarrow Sn}$ is particularly evident for the def2-SVPD basis set whose diffuse functions shorten the $d_{N\rightarrow Sn}$ distance by 0.222 Å. On the other hand, the difference between the $d_{N\rightarrow Sn}$ value obtained using def2-QZVPP and the $d_{N\rightarrow Sn}$ value yielded by def2-QZVPPD is minor (<0.01 Å). For Dunning's basis sets, the effect of diffuse functions on $d_{N\rightarrow Sn}$ seems to be more systematic as it gives a decrease of 0.100–0.145 Å for $X = D$, T, Q. The irregularity of the effect of diffuse functions in the def2-*Y*(Z)VP(P)D basis sets on $d_{N\rightarrow Sn}$ may be due to the fact that the diffuse functions included in def2-*Y*(Z)VP(P)D were primarily designed to achieve high accuracy for molecular polarizabilities. Unfortunately, the diffuse functions included in def2-QZVPPD turn out to be inappropriate for predicting $d_{N\rightarrow Sn}$. The value of $d_{N\rightarrow Sn}$ obtained using def2-QZVPPD deviates from that yielded by aug-cc-pVQZ significantly, whereas def2-QZVPP and cc-pVQZ lead to similar values of $d_{N\rightarrow Sn}$. In order to check whether it is possible to construct a diffuse-augmented def2-QZVPP that converges to aug-cc-pVQZ, we considered four additional diffuse augmentation schemes for def2-QZVPP. The first one was the minimal augmentation scheme proposed by Truhlar and co-workers [74] and the other three combined def2-QZVPP with the sets of diffuse functions taken directly from aug-cc-pV*X*Z, where $X = T$, Q, 5. The resulting basis sets, namely ma-def2-QZVPP, aug-T-def2-QZVPP, aug-Q-def2-QZVPP, and aug-5-def2-QZVPP, respectively, lead to the $d_{N\rightarrow Sn}$ values that are lower than that obtained using def2-QZVPPD. On the other hand, the minimal augmentation scheme does not provide any

improvement in $d_{N\rightarrow Sn}$ over the regular def2-QZVPP basis set. The aug-*X*-def2-QZVPP basis sets perform considerably better and they offer a systematic improvement in $d_{N\rightarrow Sn}$. Their $d_{N\rightarrow Sn}$ values are indeed much lower than that of def2-QZVPPD and, what is more important, than that of def2-QZVPP. The $d_{N\rightarrow Sn}$ distance obtained using aug-Q-def2-QZVPP remains longer by 0.065 Å than that yielded by aug-cc-pVQZ although the sizes of both basis sets are similar (ca. 2250 Gaussian primitives for the whole dimer). The enlargement of the diffuse function set from aug-Q to aug-5 leads to a negligible decrease in the length of $d_{N\rightarrow Sn}$, which suggests that the limit for def2-QZVPP augmented with the 'aug' sets is practically reached. Thus, we can conclude that the difference of ca. 0.06 Å is inherent in the best estimates of $d_{N\rightarrow Sn}$ obtained from Ahlrichs' and Dunning's families of basis sets. Table 3 presents the RMSD values calculated for $(Me_3SnCN)_2$ optimized by SCS-MP2 in combination with all considered basis sets with respect to the $(Me_3SnCN)_2$ geometry obtained using SCS-MP2/aug-cc-pVQZ. The tabulated values demonstrate the basis set effects that mimic those discussed for the $d_{N\rightarrow Sn}$ parameter. It obviously indicates the importance of this geometrical parameter in characterizing the intermolecular N → Sn coordination and in predicting the geometry of the whole $(Me_3SnCN)_2$ dimer reliably. It also confirms that the most economical diffuse augmentation scheme applied to the def2-QZVPP basis set is not a satisfactory alternative to the 'aug' sets of diffuse functions for predicting the geometry of $(Me_3SnCN)_2$.

**Table 2** Selected distances and angle in $(Me_3SnCN)_2$ optimized by SCS-MP2 in conjunction with various basis sets

| Basis set | $d_{N\rightarrow Sn}$ | $d_{C\equiv N}$ | $d_{Sn-CN}$ | $d_{Sn-CH_3}$ | $a_{N\rightarrow Sn-CH_3}$ |
|---|---|---|---|---|---|
| cc-pVDZ | 3.100 | 1.186 | 2.180 | 2.153 | 78.50 |
| cc-pVTZ | 3.129 | 1.172 | 2.161 | 2.135 | 78.18 |
| cc-pVQZ | 3.076 | 1.169 | 2.150 | 2.120 | 78.51 |
| aug-cc-pVDZ | 2.955 | 1.187 | 2.195 | 2.152 | 79.83 |
| aug-cc-pVTZ | 3.029 | 1.172 | 2.165 | 2.130 | 78.95 |
| aug-cc-pVQZ | 2.964 | 1.169 | 2.151 | 2.116 | 79.18 |
| def2-SVP | 3.159 | 1.179 | 2.181 | 2.153 | 78.19 |
| def2-TZVPP | 3.149 | 1.171 | 2.154 | 2.126 | 78.16 |
| def2-QZVPP | 3.098 | 1.169 | 2.151 | 2.122 | 78.36 |
| def2-SVPD | 2.937 | 1.180 | 2.193 | 2.153 | 79.48 |
| def2-TZVPPD | 3.093 | 1.172 | 2.156 | 2.127 | 78.51 |
| def2-QZVPPD | 3.107 | 1.169 | 2.151 | 2.122 | 78.31 |
| ma-def2-QZVPP | 3.100 | 1.169 | 2.151 | 2.122 | 78.35 |
| aug-T-def2-QZVPP | 3.052 | 1.169 | 2.154 | 2.121 | 78.66 |
| aug-Q-def2-QZVPP | 3.029 | 1.170 | 2.154 | 2.120 | 78.99 |
| aug-5-def2-QZVPP | 3.021 | 1.170 | 2.150 | 2.119 | 78.95 |

Distances in Å, angle in °

These distances and this angle are marked in Fig. 2

**Table 3** RMSD for the $(Me_3SnCN)_2$ geometries obtained by SCS-MP2 combined with various basis sets with respect to the $(Me_3SnCN)_2$ geometry optimized using SCS-MP2/aug-cc-pVQZ

| Basis set | RMSD |
|---|---|
| cc-pVDZ | 9.795 |
| cc-pVTZ | 8.210 |
| cc-pVQZ | 5.095 |
| aug-cc-pVDZ | 5.490 |
| aug-cc-pVTZ | 3.924 |
| aug-cc-pVQZ | 0.000 |
| def2-SVP | 11.873 |
| def2-TZVPP | 8.412 |
| def2-QZVPP | 5.977 |
| def2-SVPD | 4.639 |
| def2-TZVPPD | 6.131 |
| def2-QZVPPD | 6.577 |
| ma-def2-QZVPP | 6.089 |
| aug-T-def2-QZVPP | 3.941 |
| aug-Q-def2-QZVPP | 2.919 |
| aug-5-def2-QZVPP | 2.433 |

All values in $10^{-2}$ Å

Let us finish the discussion of the $(Me_3SnCN)_2$ geometry by comparing the geometrical parameters in the dimer optimized using SCS-MP2/aug-cc-pVQZ with the crystal structure of trimethyltin cyanide determined by Avalle et al. [12]. In the crystalline trimethyltin cyanide, the linear chains of $Me_3SnCN$ molecules possess the $C_3Sn$ fragments exhibiting the eclipsed arrangement. Such an arrangement also turns out to be the most stable for the dimer. In the preliminary stage of our investigation of $(Me_3SnCN)_2$ we considered its several possible geometrical configurations (those that are energetic local minima are depicted in Fig. 3) and the configuration with two $C_3Sn$ fragments in the eclipsed arrangement exhibited the lowest total energy (see Table 4). Therefore, the results discussed both in the above paragraphs and further in this section were obtained for this geometrical configuration of $(Me_3SnCN)_2$. Our calculations indicate that the geometry around the Sn atom of **2** is a distorted trigonal bipyramid. The distortion of geometry around pentacoordinated Sn atom from trigonal bipyramidal is common to $(Me_3SnCN)_2$ and the crystalline trimethyltin cyanide. The $a_{N\rightarrow Sn-CH_3}$ angle is an indicator of such a distortion and its values are smaller than 90° both in the dimer and in the crystal (the ideal trigonal bipyramid around the Sn atom exhibits the $a_{N\rightarrow Sn-CH_3}$ angle equal to 90°). More specifically, the X-ray single-crystal diffraction measurement [12] indicated that each $C_3Sn$ fragment in the linear chains of $Me_3SnCN$ molecules was not strictly planar because the Me groups were bent toward a more distant atom, most probably the N atom of the neighboring

$Me_3SnCN$ molecule. Our calculations confirm the bend of all three Me groups toward the N atom being the Lewis base center. However, the distortion from the trigonal bipyramid is larger in the dimer than in the crystal. This larger distortion in the dimer is associated with longer intermolecular $d_{N\rightarrow Sn}$ distance. The longer $d_{N\rightarrow Sn}$ distance shifts the geometry around the Sn atom of **2** toward the tetrahedral geometry. Nevertheless, the value of $d_{N\rightarrow Sn}$ is still much smaller than the sum of the N-atom and Sn-atom van der Waals radii (2.42 Å for Sn and 1.66 Å for N [75]). The compression of $d_{N\rightarrow Sn}$ in the crystal is obviously due to the presence of more distant $Me_3SnCN$ molecules belonging to the same polymeric chain. The compression of $d_{N\rightarrow Sn}$ results in the elongation of the distance between the Sn atom and the C atom of the cyano group, $d_{Sn-CN}$. The triple bond in the cyano group is rigid and does not undergo any significant change while one goes from the dimer to the crystal. Similarly, the bond lengths between the Sn atom and the C atoms of Me groups remain very similar in the crystal and in the dimer. Some possible lateral interactions between the neighboring chains of $Me_3SnCN$ molecules in the crystal would primarily affect the inner geometry of Me groups. The similar values of $d_{Sn-CH_3}$ in the dimer and in the crystal imply that the geometrical parameters describing the intermolecular N → Sn coordination in each chain of $Me_3SnCN$ molecules are influenced by the surrounding chains only minimally. To conclude this part of the discussion, many structural features characterizing the intermolecular N → Sn coordination in $(Me_3SnCN)_2$ are analogous to those observed in the crystalline trimethyltin cyanide. However, $d_{N\rightarrow Sn}$ in the dimer is elongated by ca. 0.36 Å compared to the $d_{N\rightarrow Sn}$ distance measured in the crystal structure. It was proven experimentally that many classical dative bonds are longer in gas-phase complexes than in the solid state and the resulting elongations may be as significant as in our case [76]. The intermolecular nature of a dative bond may also contribute to its significant elongation. The elongation of $d_{N\rightarrow Sn}$ in $(Me_3SnCN)_2$ is much larger than the elongations reported for intramolecular O → Sn bonds [77, 78].

Next, we will focus on the counterpoise-corrected interaction energy $E_{int}$ between the $Me_3SnCN$ molecules in the dimer optimized at the SCS-MP2/aug-cc-pVQZ level of theory. The values of $E_{int}$ were calculated using the MP2, SCS-MP2, CCSD, and CCSD(T) methods in conjunction with four sequences of basis sets. These values, together with the corresponding BSSEs, are listed in Table 5. Some values are missing there because performing CCSD and CCSD(T) calculations with basis sets larger than those of triple-ζ quality turned out to be too time-, memory-, and disk space-consuming for the computer system available to us. The CCSD(T) method is considered to be the "golden standard" for obtaining accurate energies

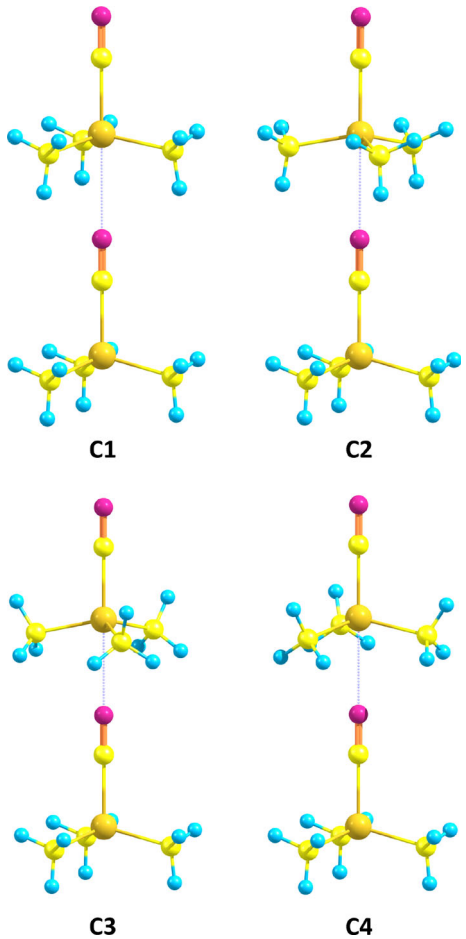


**Fig. 3** Geometrical configurations of $(Me_3SnCN)_2$. Individual atoms are represented by the *same colors* as in Fig. 2 (Color figure online)

of weak molecular interactions [79] and we also designate this method as that providing the reference values of $E_{int}$ in $(Me_3SnCN)_2$. In each sequence of basis sets, the MP2 method overestimates the strength of the interaction between two $Me_3SnCN$ molecules because the $E_{int}$ values yielded by MP2 are more negative than the reference CCSD(T) results. The MP2 values of $E_{int}$ exceed those calculated using CCSD(T) by 11 % at the most. It is due to the fact that MP2 includes only the uncoupled Hartree–Fock dispersion energy that is known to be overestimated. The overestimation of $E_{int}$ in $(Me_3SnCN)_2$ is, however, smaller than that reported for various dispersion-bound complexes [80, 81]. The SCS-MP2 and CCSD methods lead to the $E_{int}$ values that are less negative than those of CCSD(T) and thus they underestimate the strength of the interaction in the dimer. Of these two methods, the SCS-MP2 one performs better and its underestimation of $E_{int}$ amounts to several percent of $E_{int}$ calculated by CCSD(T). It is worth noting that SCS-MP2 is considerably less expensive than CCSD. In each sequence of basis sets, the enlargement of the basis set from double- to triple-ζ quality

**Table 4** Selected distances and angle in four geometrical configurations of $(Me_3SnCN)_2$ optimized at the SCS-MP2/aug-cc-pVQZ level of theory

| $(Me_3SnCN)_2$ configuration | $d_{N\rightarrow Sn}$ | $d_{C\equiv N}$ | $d_{Sn-CN}$ | $d_{Sn-CH_3}$ | $a_{N\rightarrow Sn-CH_3}$ | $\Delta E$ |
|---|---|---|---|---|---|---|
| C1 | 2.964 | 1.169 | 2.151 | 2.116 | 79.18 | 0.0000 |
| C2 | 2.965 | 1.169 | 2.151 | 2.116 | 79.17 | 0.0130 |
| C3 | 2.843 | 1.169 | 2.153 | 2.118 | 77.86 | 0.0133 |
| C4 | 2.839 | 1.168 | 2.153 | 2.118 | 77.86 | 0.0177 |
| Crystal [12] | 2.607 | 1.127 | 2.295 | 2.134 | 84.11 | |

Distances in Å, angle in ° and energy differences in kcal/mol

These geometrical configurations are denoted the same as in Fig. 3 and are ordered with respect to the energy of the most stable configuration, $\Delta E$. The distances and the angle are marked in Fig. 2

results in the greatest change in $E_{int}$. This change is particularly evident for two sequences of basis sets without diffuse functions, that is, cc-pV*X*Z and def2-*Y*(Z)VP(P). For the former the change in $E_{int}$ amounts up to 1.52 kcal/mol, whereas the enlargement from cc-pVQZ to cc-pV5Z increases the strength of the interaction only by ca. 0.2 kcal/mol. The cc-pV5Z basis set is saturated enough and the addition of diffuse functions to this basis set leads to a change of merely ca. 0.1 kcal/mol in $E_{int}$. In contrast to it, the addition of diffuse functions to cc-pVDZ and def2-SVP is necessary to obtain the $E_{int}$ value with satisfactory accuracy. It is noteworthy that, of triple- and quadruple-ζ basis sets without diffuse functions, the family of Ahlrichs' basis sets performs better than the family of Dunning's basis sets. For instance, the comparison of the $E_{int}$ values obtained by cc-pVQZ and by def2-QZVPP with the corresponding $E_{int}$ calculated using cc-pV5Z reveals that the $E_{int}$ values provided by def2-QZVPP are closer to those of cc-pV5Z. As it can be seen in Table 5, the values of the BSSE are generally significant for all basis sets and the omission of the counterpoise correction for the BSSE would deteriorate to a large extent the accuracy of the calculated $E_{int}$ values. Particularly severe overestimation of the strength of the interaction could be observed for def2-SVP and def2-SVPD where the correction for the BSSE decreases the strength of the interaction by ca. 40 %. Another effect degrading the quality of the predicted $E_{int}$ values is the basis-set incompleteness. In order to get rid of this effect, we extrapolated the $E_{int}$ values to the CBS limit. The CBS(2,3) extrapolation scheme was based on the energies calculated using double- and triple-ζ basis sets. Additionally, the energies obtained using triple- and quadruple-ζ basis sets were adopted to extrapolate $E_{int}$ at the MP2 and SCS-MP2 levels of theory (the respective scheme is denoted by CBS(3,4) in Table 5). The application of the CBS(2,3) scheme allows the MP2 and SCS-MP2 methods to predict the $E_{int}$ values that are close to those obtained using quadruple- or even quintuple-ζ basis sets. When the $E_{int}$ values obtained from MP2/CBS(2,3) and SCS-MP2/CBS(2,3) are compared with the $E_{int}$ values determined at the CCSD(T)/CBS(2,3) level, it is evident that the performance of MP2/CBS(2,3) and SCS-MP2/CBS(2,3) is almost identical in the sense that the former overestimates, whereas the latter underestimates the CCSD(T)/CBS(2,3) strength of the interaction by similar values (ca. 0.5 kcal/mol). It can be observed for all four sequences of basis sets. The CCSD(T) method combined with the extrapolation scheme using the aug-cc-pV*X*Z with $X = D, T$ provides the $E_{int}$ value of −7.64 kcal/mol and we designate this value as the most accurate estimation of $E_{int}$ in $(Me_3SnCN)_2$. For each method, its $E_{int}$ value extrapolated by the CBS(2,3) scheme varies noticeably, while going from one sequence of basis sets to another. A good agreement in the extrapolated $E_{int}$ values obtained by a given method with all four sequences of basis sets can be reached by using the CBS (3,4) scheme. Unfortunately, we are able to prove the aforementioned finding only for MP2 and SCS-MP2. Nevertheless, such a finding deserves attention in the case of Ahlrichs' basis sets because they were very rarely used to extrapolate interaction energies [82]. Moreover, from the computational point of view the fact that the difference in interaction energies extrapolated using def2-*Y*ZVPPD with $Y = T, Q$ and using aug-cc-pV*X*Z with $X = T, Q$ vanishes is important because the smaller number of basis functions in def2-*Y*ZVPPD (compared to the number of basis functions in aug-cc-pV*X*Z) allows us to achieve significant computational savings without loss of accuracy.

Our calculations of $E_{int}$ in $(Me_3SnCN)_2$ indicate that the interaction between the $Me_3SnCN$ molecules is small and thus the N → Sn coordination bond in this dimer is weak. More specifically, it is several times weaker than the classic dative bonds. For instance, the N → B bond energy in ammonia borane, which is a well-known prototype of dative bond, is estimated to be 37.5 kcal/mol [83]. The weak N → Sn interaction in $(Me_3SnCN)_2$ is accompanied by the large $d_{N\rightarrow Sn}$ distance, although it should be noted that in the case of dative bonds their strength and length do not always display a straightforward relation [84].

As the next stage of our investigation, the intermolecular N → Sn coordination will be analyzed through its bonding

**Table 5** $E_{int}$ between the $Me_3SnCN$ molecules in $(Me_3SnCN)_2$ and the corresponding BSSE (in parentheses)

| Basis set | Method | | | |
|---|---|---|---|---|
| | MP2 | SCS-MP2 | CCSD | CCSD(T) |
| cc-pVDZ | −5.51 (−3.90) | −4.77 (−3.75) | −4.67 (−3.64) | −4.94 (−3.91) |
| cc-pVTZ | −7.03 (−1.84) | −6.02 (−1.77) | −5.91 (−1.68) | −6.41 (−1.82) |
| cc-pVQZ | −7.77 (−1.22) | −6.65 (−1.16) | | |
| cc-pV5Z | −8.00 (0.56) | −6.85 (0.53) | | |
| CBS(2,3) | −7.67 | −6.54 | −6.43 | −7.02 |
| CBS(3,4) | −8.26 | −7.05 | | |
| aug-cc-pVDZ | −7.23 (−3.50) | −6.14 (−3.45) | −6.11 (−3.38) | −6.67 (−3.62) |
| aug-cc-pVTZ | −7.87 (−2.59) | −6.72 (−2.53) | −6.69 (−2.38) | −7.36 (−2.50) |
| aug-cc-pVQZ | −8.08 (−2.45) | −6.92 (−2.28) | | |
| aug-cc-pV5Z | −8.13 (−2.06) | −6.97 (−1.85) | | |
| CBS(2,3) | −8.13 | −6.95 | −6.92 | −7.64 |
| CBS(3,4) | −8.22 | −7.05 | | |
| def2-SVP | −5.34 (−3.87) | −4.68 (−3.72) | −4.60 (−3.60) | −4.84 (−3.88) |
| def2-TZVPP | −7.20 (−1.19) | −6.16 (−1.17) | −6.04 (−1.07) | −6.55 (−1.19) |
| def2-QZVPP | −7.89 (−0.77) | −6.72 (−0.77) | | |
| CBS(2,3) | −7.99 | −6.80 | −6.66 | −7.29 |
| CBS(3,4) | −8.38 | −7.17 | | |
| def2-SVPD | −7.10 (−5.53) | −6.05 (−5.41) | −6.02 (−5.40) | −6.55 (−5.73) |
| def2-TZVPPD | −7.60 (−1.68) | −6.49 (−1.70) | −6.41 (−1.52) | −7.01 (−1.65) |
| def2-QZVPPD | −7.98 (−0.98) | −6.82 (−0.99) | | |
| CBS(2,3) | −7.80 | −6.66 | −6.55 | −7.19 |
| CBS(3,4) | −8.23 | −7.05 | | |

All values in kcal/mol

The BSSE correction is included in the values of $E_{int}$

characteristics provided by several theoretical tools with great interpretative potential. Similarly to the determination of $E_{int}$ in the previous paragraphs, the following analysis will be carried out for the geometry of $(Me_3SnCN)_2$ optimized by SCS-MP2/aug-cc-pVQZ.

For a better understanding of the character of the N → Sn interaction in $(Me_3SnCN)_2$, we calculated the value of $E_{int}$ in the dimer using SAPT. SAPT represents $E_{int}$ as a series of energy correction terms that include various, and often very subtle, energetic effects required to reproduce intermolecular interactions accurately. In addition to the calculation of the $E_{int}$ value as such, the energy correction terms present in SAPT provided a means of the intuitive analysis of $E_{int}$ on the basis of physically meaningful components. Table 6 shows the SAPT energy correction terms determined for the interaction between the $Me_3SnCN$ molecules in $(Me_3SnCN)_2$. The explanation of the notation used for these terms, as well as their physical meaning, can be found in the review paper by Jeziorski et al. [63] and in the documentation freely available on the SAPT web page [85]. Our SAPT calculation made use of the modest aug-cc-pVDZ basis set due to the fact that computing some SAPT energy correction terms, such as $\varepsilon_{disp}^{(2)}(2)$, was very demanding (other details of the SAPT calculation are described in Section S3, Electronic supplementary material). Although the basis set was modest, SAPT predicts the value of $E_{int}$ in excellent accordance with the extrapolated CCSD(T) value. It is worth noting that $E_{int}$ obtained from SAPT is inherently free from the BSSE. The inclusion of the $\delta E_{int,resp}^{HF}$ term turned out to be necessary to calculate $E_{int}$ with great accuracy. As a matter of fact, the inclusion of $\delta E_{int,resp}^{HF}$ in $E_{int}$ is recommended if pseudopotentials are used within SAPT [86]. As it can be seen in Table 6, the $E_{elst}^{(10)}$ term is the largest attractive term. This term covers the Coulombic interactions between the permanent multipole moments of the $Me_3SnCN$ molecules. The $Me_3SnCN$ molecule possesses a significant dipole moment of 4.99 D and in $(Me_3SnCN)_2$ the oppositely charged centers belonging to different molecules are in their immediate neighborhood (the analysis of atomic charges will be reported further in this work), which results in the significant electrostatic attraction between the $Me_3SnCN$ molecules. The induction term $E_{ind,resp}^{(20)}$ is substantially quenched by its exchange counterpart

$E^{(20)}_{\text{exch-ind,resp}}$ and thus the induction at the uncorrelated level constitutes a relatively small contribution to $E_{\text{int}}$. The $\delta E^{\text{HF}}_{\text{int,resp}}$ value of −0.87 kcal/mol indicates that higher order induction and exchange energy correction terms have a small effect on $E_{\text{int}}$. The sum of the uncorrelated terms $\left(E^{(10)}_{\text{elst}} + E^{(10)}_{\text{exch}} + E^{(20)}_{\text{ind,resp}} + E^{(20)}_{\text{exch-ind,resp}}\right)$ amounts to merely −2.48 kcal/mol, so the terms accounting for inter- and intramolecular electron correlation effects need to be included in order to predict $E_{\text{int}}$ properly. Of the correlated terms, the dispersion one $E^{(20)}_{\text{disp}}$ corresponds to the most attractive force. The value of the $E^{(20)}_{\text{disp}}$ energy is approximately comparable to that of the $E^{(20)}_{\text{ind,resp}}$ term but the $E^{(20)}_{\text{disp}}$ energy is quenched by $E^{(20)}_{\text{exch-disp}}$ to a much lesser extent than $E^{(20)}_{\text{ind,resp}}$ is by $E^{(20)}_{\text{exch-ind,resp}}$. It is possible to group the SAPT energy correction terms into four principal components representing electrostatic, exchange, induction, and dispersion contributions to $E_{\text{int}}$: $E_{\text{elst}}$, $E_{\text{exch}}$, $E_{\text{ind}}$ and $E_{\text{disp}}$, respectively. Then, one can notice that $E_{\text{exch}}$ is not compensated by $E_{\text{elst}}$ and the addition of $E_{\text{ind}}$ to the $E_{\text{exch}}$ and $E_{\text{elst}}$ components leads to a negligible stabilization of the dimer (−0.10 kcal/mol). Comparing this value with the value of $E_{\text{int}}$ allows us to stress once again the importance of dispersion in the stabilization of $(Me_3SnCN)_2$. The dominant role of dispersion is generally a typical feature of interactions in weak non-bonded complexes, e.g., in a complex of Ar with $H_2$ [63]. The small value of $E_{\text{int}}$ and the relatively long $d_{\text{N}\rightarrow\text{Sn}}$ distance in $(Me_3SnCN)_2$ seem to make the SAPT characteristics of the interaction in this dimer resemble that of weak non-bonded complexes. On the other hand, the important role of dispersion should not be restricted only to weak non-bonded complexes. For instance, it was shown by Zahn et al. [87] using SAPT that dispersion interactions, together with induction ones are responsible for essential physicochemical properties of an imidazolium-based ionic liquid. In the case of complexes with dative bonds, the induction energy is often more stabilizing than the dispersion component, as it was reported for $NH_3 \rightarrow BH_3$ and $NMe_3 \rightarrow BH_3$ [88]. The interaction in these two complexes is, however, much stronger than that in $(Me_3SnCN)_2$. On this basis, it can be expected that the significance of the $E_{\text{disp}}$ component in the stabilization of complexes with a coordination bond grows when the intermolecular interaction becomes weaker and weaker.

In the subsequent part of this work, we continue with the discussion of the chemical bonding in $(Me_3SnCN)_2$ in terms of energetic quantities and we will inspect the donor–acceptor (or charge transfer, CT) interactions occurring between the $Me_3SnCN$ molecules and leading to the energetic stabilization of the dimer. Within the framework of the NBO analysis, the donor–acceptor interactions are associated with the occupancy shifts from the filled NBOs (that is, the donor NBOs) of one $Me_3SnCN$ molecule to the unfilled NBOs (that is, the acceptor NBOs) of another $Me_3SnCN$ molecule and the stabilization energies $\Delta E^{(2)}$ resulting from these interactions can be estimated using a standard second-order perturbation treatment [65]. The details of the leading intermolecular donor–acceptor interactions in $(Me_3SnCN)_2$ are summarized in Table 7. The tabulated results were obtained using the aug-cc-pVTZ basis set. For each interaction, the table shows the respective donor and acceptor NBOs, the occupancy of the acceptor NBO, and the $\Delta E^{(2)}$ value corresponding to this interaction. Although only the most important intermolecular donor–acceptor interactions are presented, many of them exhibit very small $\Delta E^{(2)}$ values (>−0.5 kcal/mol). It is not surprising because the strength of the interaction between the $Me_3SnCN$ molecules is generally small, as it was demonstrated by $E_{\text{int}}$. The donor–acceptor interaction between the σ-type lone pair on the N atom of **1** and the antibonding $\sigma^*$(Sn–CN) orbital of **2** gives the principal stabilization and the resulting $\Delta E^{(2)}$ value is equal to −6.35 kcal/mol (the contour plots of both NBOs involved in this interaction are drawn in Fig. S1, Electronic supplementary material). This value is, however, very small compared to the donor–acceptor stabilization observed for many dative bonds with tin [13, 89, 90]. The donor–acceptor interaction between the N-atom lone pair and the σ*(Sn–$CH_3$) orbital of **2** provides the stabilization of merely −1.19 kcal/mol but

**Table 6** SAPT energy correction terms, collective components corresponding to four principal forces and $E_{\text{int}}$ obtained from SAPT

| Energy | Value |
|---|---|
| $E^{(10)}_{\text{elst}}$ | −12.23 |
| $E^{(10)}_{\text{exch}}$ | 12.39 |
| $E^{(20)}_{\text{ind,resp}}$ | −6.27 |
| $E^{(20)}_{\text{exch-ind,resp}}$ | 3.63 |
| $\varepsilon^{(1)}_{\text{elst,resp}}(3)$ | 0.07 |
| $\varepsilon^{(1)}_{\text{exch}}(\text{CCSD})$ | 2.71 |
| ${}^{\text{t}}E^{(22)}_{\text{ind}}$ | −0.93 |
| ${}^{\text{t}}E^{(22)}_{\text{exch-ind}}$ | 0.54 |
| $E^{(20)}_{\text{disp}}$ | −7.46 |
| $\varepsilon^{(2)}_{\text{disp}}(2)$ | −0.18 |
| $E^{(20)}_{\text{exch-disp}}$ | 1.04 |
| $\delta E^{\text{HF}}_{\text{int,resp}}$ | −0.87 |
| $E_{\text{elst}}$ | −12.16 |
| $E_{\text{exch}}$ | 15.10 |
| $E_{\text{ind}}$ | −3.04 |
| $E_{\text{disp}}$ | −6.61 |
| $E_{\text{int}}$ | −7.57 |

All values in kcal/mol

**Table 7** Intermolecular donor–acceptor interactions in $(Me_3SnCN)_2$

| Donor NBO | Acceptor NBO | Acceptor NBO occupancy | $\Delta E^{(2)}$ |
|---|---|---|---|
| **1 → 2** | | | |
| BD(N–C) $sp^{1.02}$–$sp^{1.15}$ | BD*(Sn–CN)[a] $sp^{5.47}$–$sp^{0.79}$ | 0.0678 | −0.68 |
| BD(N–C) $sp^{1.02}$–$sp^{1.15}$ | BD*(Sn–$CH_3$)[b] $sp^{2.53}$–$sp^{3.30}$ | 0.0508 | −0.06 |
| BD(N–C) $sp^{1.02}$–$sp^{1.15}$ | RY*(Sn) | 0.0009 | −0.40 |
| LP(N) $sp^{0.95}$ | BD*(Sn–CN)[a] $sp^{5.47}$–$sp^{0.79}$ | 0.0678 | −6.35 |
| LP(N) $sp^{0.95}$ | BD*(Sn–$CH_3$)[b] $sp^{2.53}$–$sp^{3.30}$ | 0.0508 | −1.19 |
| LP(N) $sp^{0.95}$ | RY*(Sn) | 0.0001 | −0.22 |
| **2 → 1** | | | |
| BD(Sn–$CH_3$)[b] $sp^{2.53}$–$sp^{3.30}$ | BD*(N–C) $sp^{1.02}$–$sp^{1.15}$ | 0.0077 | −0.18 |
| BD(Sn–CN)[a] $sp^{5.47}$–$sp^{0.79}$ | RY*(N) | 0.0013 | −0.06 |
| BD(Sn–$CH_3$)[b] $sp^{2.53}$–$sp^{3.30}$ | RY*(N) | 0.0013 | −0.26 |

$\Delta E^{(2)}$ values in kcal/mol, the occupancy of acceptor NBOs in *e*

The following notation is used for NBOs: BD and BD* are two-center bonding and antibonding orbitals, respectively; LP is a valence lone electron pair; RY* is an extra-valence-shell orbital. Hybridization of natural hybrid orbitals forming BD, BD* and LP is also shown

[a] 'CN' indicates the constituent natural hybrid orbital on the C atom of cyano group

[b] '$CH_3$' indicates the constituent natural hybrid orbital on the C atom of methyl group

the same stabilization can be found for the NBOs involving each of the other two methyl carbons in **2**. The intermolecular donor–acceptor interactions are also observed between the donor NBOs of **2** and the acceptor NBOs of **1** but their stabilization energies are obviously much smaller.

The interaction between the $Me_3SnCN$ molecules leads to a redistribution of electron charge in the dimer. There is a minor electron CT from **1** to **2**. Our estimate of the CT between the $Me_3SnCN$ molecules amounts to 0.016–0.030*e* (see $Q$ in Table 8) and is based on atomic charges summed for all atoms in each $Me_3SnCN$ molecule of the dimer. The $Q$ quantity calculated in that fashion seems to be a relatively reliable measure of CT between molecules linked through a dative bond [84]. Regardless of whether natural population analysis (NPA) atomic charges or QTAIM atomic charges are used, our estimated values of $Q$ are very small. A very little CT was also reported for the HCN → $BF_3$ complex whose $E_{int}$ is similar to that of $(Me_3SnCN)_2$ (although the N → B distance is much shorter) [84]. The direction of CT

**Table 8** CT between the $Me_3SnCN$ molecules in the dimer and selected atomic charges obtained from the NPA and QTAIM analyses

| | NPA | QTAIM |
|---|---|---|
| $Q$ | 0.030 | 0.016 |
| $q$(N)[a] | −0.407 | −1.219 |
| $q$(Sn)[b] | 1.649 | 1.831 |

All values in *e*

[a] The N atom of **1**

[b] The Sn atom of **2**

agrees qualitatively with the results gathered in Table 7. The occupancies of the acceptor NBOs on **2** are larger than those of the acceptor NBOs on **1**, which may suggest the direction of CT (one should, however, remember that only selected intermolecular donor–acceptor interactions are presented in Table 7). Table 8 also presents the NPA and QTAIM atomic charges $q$ on the N atom of **1** and on the Sn atom of **2**. The magnitude of $q$(N) obtained from the NPA varies considerably from that calculated using the QTAIM method. This should not be completely surprising because it is known that various population analysis schemes may lead to significantly different results even for the simplest molecules [91]. Nevertheless, both the NPA and QTAIM atomic charges clearly indicate that there is a significant accumulation of electron charge on the N atom of **1**, whereas the electron charge of 1.65–1.83*e* outflows from the Sn atom of **2**. The occurrence of such oppositely charged centers results in the mostly ionic character of the N → Sn coordination bond.

Additional insight into the intermolecular N → Sn interaction can be obtained from the full topological analysis of the electron density distribution $\rho(\mathbf{r})$ of the dimer. The values of $\rho(\mathbf{r})$ were calculated at the SCS-MP2/aug-cc-pVTZ level of theory and then $\rho(\mathbf{r})$ was analyzed within the framework of the QTAIM. The QTAIM analysis indicates the presence of a (3, −1) critical point between the N atom of **1** and the Sn atom of **2** (see Fig. 4). The corresponding bond path links this bond critical point with two (3, −3) critical points located at the N and Sn atoms. This provides evidence that, from the QTAIM viewpoint, these two atoms are bonded to one another [92]. The values of selected QTAIM parameters at the above-mentioned bond critical point are listed in Table 9. These values indicate the "closed-shell" nature of the N → Sn interaction [93]. The value of $\rho(\mathbf{r})$ is small and the Laplacian $\nabla^2\rho(\mathbf{r})$ is positive, which means that there is an electron charge contraction away from the interatomic region between the N and Sn atoms toward these two atoms. The small value of $\rho(\mathbf{r})$ is expected as the $d_{N\rightarrow Sn}$ distance is large and the strength of the interaction between the $Me_3SnCN$ molecules is minor. The positive values of $\nabla^2\rho(\mathbf{r})$ were often found at the bond critical point between atoms involved in dative bonds [84,

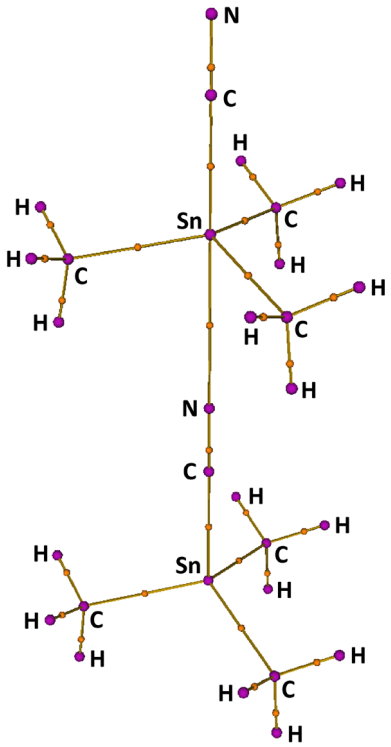


**Fig. 4** Molecular graph of $(Me_3SnCN)_2$. The (3, −3) critical points that are found in nuclear positions are denoted by *violet circles*, whereas *orange circles* correspond to the (3, −1) critical points linked with the (3, −3) critical points by bond paths that are in turn *colored olive* (Color figure online)

94] including the intramolecular N → Sn [95] and O → Sn [78] bonds. The electron kinetic energy density $G(\mathbf{r})$ outweighs the electron potential energy density $V(\mathbf{r})$, resulting in the positive sign of the electron energy density $H(\mathbf{r}) = G(\mathbf{r}) + V(\mathbf{r})$. The positive sign of $H(\mathbf{r})$ suggests that the $Me_3SnCN$ molecules are held together by electrostatic interactions. Finally, the ratios $-V(\mathbf{r})/G(\mathbf{r}) < 1$ and $-\lambda_1/\lambda_3 < 1$ (where $\lambda_1$ and $\lambda_3$ are the lowest and highest eigenvalues of the Hessian matrix of $\rho(\mathbf{r})$, respectively) also point to the "closed-shell" character of the N → Sn interaction in $(Me_3SnCN)_2$ [66, 93].

The intermolecular N → Sn interaction in $(Me_3SnCN)_2$ can also be characterized using the analysis of ELF in the dimer. Figure 5 depicts ELF valence domains in $(Me_3SnCN)_2$. There is only one ELF valence domain in the region between the N atom of **1** and the Sn atom of **2**. This ELF domain is adjacent to the N atom and obviously represents its lone pair. The distance between the ELF attractors corresponding to the N-atom lone pair and to the N-atom core amounts to 0.635 Å (ELF core domains are not visible in Fig. 5). The distance between the analogous attractors of the N atom in **2** is longer by 0.032 Å. The absence of any typical bonding, that is disynaptic, ELF valence domain between the N atom of **1** and the Sn atom of **2** supports the QTAIM identification of the N → Sn interaction with the "closed-shell" interaction. More specifically, both QTAIM and ELF results are in agreement with the predominant ionic character of the N → Sn interaction.

**Table 9** Selected QTAIM parameters at the bond critical point located between the N atom of **1** and the Sn atom of **2** in $(Me_3SnCN)_2$

| Parameter | Value |
|---|---|
| $\rho(\mathbf{r})$ | $1.501 \times 10^{-2}$ |
| $\nabla^2\rho(\mathbf{r})$ | $4.676 \times 10^{-2}$ |
| $G(\mathbf{r})$ | $1.083 \times 10^{-2}$ |
| $V(\mathbf{r})$ | $-9.969 \times 10^{-3}$ |
| $H(\mathbf{r})$ | $8.602 \times 10^{-4}$ |
| $-V(\mathbf{r})/G(\mathbf{r})$ | 0.920 |
| $-\lambda_1/\lambda_3$ | 0.143 |

All values in atomic units, except for the $-V(\mathbf{r})/G(\mathbf{r})$ and $-\lambda_1/\lambda_3$ ratios that are dimensionless

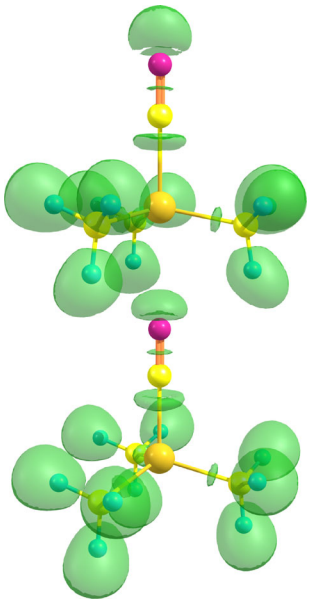

**Fig. 5** ELF isosurfaces with a contour value of 0.85 for $(Me_3SnCN)_2$. Atoms are marked with the *same colors* as in Fig. 2 (Color figure online)

Finally, it is advisable to compare the $(Me_3SnCN)_2$ dimer with the free $Me_3SnCN$ molecule in order to determine how the N → Sn coordination influences the geometrical configuration about the tin. Selected geometrical parameters of the free $Me_3SnCN$ molecule optimized at the SCS-MP2/aug-cc-pVQZ level of theory are gathered in Table 10. The coordination of the donor $Me_3SnCN$ molecule to the acceptor one leads to an elongation of the $d_{Sn-CN}$ distance bond by 0.033 Å. It is associated with an increase in the occupancy of σ*(Sn–CN) and, in consequence, the hyperconjugative effect is observed for the Sn–CN bond. Other distances in $(Me_3SnCN)_2$ demonstrate negligible changes when compared to those found in the

**Table 10** Selected distances and angle in the $Me_3SnCN$ molecule optimized using SCS-MP2/aug-cc-pVQZ

| Parameter | Value |
|---|---|
| $d_{C\equiv N}$ | 1.170 |
| $d_{Sn-CN}$ | 2.118 |
| $d_{Sn-CH_3}$ | 2.116 |
| $a_{N\rightarrow Sn-CH_3}$ [a] | 74.71 |

Distances in Å, angle in °

[a] This angle is calculated as 180° minus $a_{NC-Sn-CH_3}$

free $Me_3SnCN$ molecule. The increase in the Sn coordination from four to five has a direct influence on the geometrical configuration about the Sn atom, as measured with $a_{N\rightarrow Sn-CH_3}$. The value of $a_{N\rightarrow Sn-CH_3}$ grows by 4.47°, which means that the tetrahedral geometry about the Sn atom in the $Me_3SnCN$ molecule undergoes a distortion toward the trigonal bipyramidal geometry. It can be deduced from the values of $a_{N\rightarrow Sn-CH_3}$ that the geometrical configuration about the Sn atom in the dimer is approximately at the midpoint between the geometries of the Sn atom in the free $Me_3SnCN$ molecule and in the crystal. The aforementioned negligible variations in the $d_{Sn-CH_3}$ and $d_{C\equiv N}$ distances are accompanied by the unchanged chemical character of the $Sn-CH_3$ and C≡N bonds in the free molecule and in the dimer: the Wiberg bond indices of $Sn-CH_3$ and C≡N are almost identical before and after the N → Sn coordination occurs. In the case of Sn–CN, its Wiberg bond index decreases from 0.69 to 0.65 as a result of the formation of $(Me_3SnCN)_2$. It is worth noting that the Wiberg bond index found for N → Sn amounts to merely 0.04, which is in line with the ionic nature of N → Sn in $(Me_3SnCN)_2$. At the very end of this work, we would like to show the effect of the N → Sn coordination on the chemical shift of tin nucleus $\delta(^{119}Sn)$ because, from the experimental point of view, $^{119}Sn$ NMR spectroscopy is one of the most important tools in the structural investigations of organotin compounds [1]. The value of $\delta(^{119}Sn)$ calculated for the $Me_3SnCN$ molecule is equal to −65 ppm, whereas the dimer exhibits the $\delta(^{119}Sn)$ value of −113 ppm (details of our $^{119}Sn$ NMR calculations are given in Section S4, Electronic supplementary material). These values indicate that the $^{119}Sn$ chemical shift moves upfield (that is, its value becomes more negative) as the coordination of the Sn atom increases, which is a well-known experimental fact [1]. The upfield shift of $\delta(^{119}Sn)$ between monomeric and dimeric forms (and consequently increasing their coordination of Sn from four to five) is common to N → Sn and O → Sn. Experimental evidence for the upfield shift of $\delta(^{119}Sn)$ by 77 ppm was found for some oxathiastannolane when it changed its form from monomeric to dimeric through the O → Sn coordination [96].

## Conclusions

In this work, the N → Sn coordination in the $(Me_3SnCN)_2$ dimer has been investigated using various theoretical methods and interpretation tools. The N atom of one $Me_3SnCN$ molecule is coordinated to the Sn atom of another $Me_3SnCN$ molecule forming a dimer whose structure around the pentacoordinated Sn atom adopts a distorted trigonal bipyramidal geometry. The distance between the N and Sn atoms involved in the N → Sn coordination amounts to 2.96 Å. This rather long distance is accompanied by a small value of the $E_{int}$ between the $Me_3SnCN$ molecules in the dimer. The results presented in this work provide new insights into the methodological aspect of the theoretical investigations of N → Sn coordination and into the theoretical characterization of the N → Sn coordination occurring in $(Me_3SnCN)_2$. Taking into account all of the above results, we make the following findings:

1. Of various MP2-based methods, the SCS-MP2 variant reproduces most accurately the reference geometry of $(Me_3SnCN)_2$ obtained at the CCSD level of theory. The accuracy of SCS-MP2 is very close to that of MP4 (SDQ) but achieved at a fraction of the computational cost required by the latter. SCS-MP2 also outperforms the conventional MP2 method in reproducing the reference geometry of $(Me_3SnCN)_2$.
2. The geometry of $(Me_3SnCN)_2$ is affected by the basis set employed. When the size of the basis set employed grows, the structural parameters describing the inner geometries of the $Me_3SnCN$ molecules in the dimer exhibit regular, monotonous changes. The basis sets belonging to both Dunning's family of basis sets and Ahlrichs' family of basis sets yield consistent values of these parameters provided that such basis sets are sufficiently large. The trends in the structural parameters characterizing the arrangement of the $Me_3SnCN$ molecules in the dimer are less regular. Furthermore, the values of the intermolecular $d_{N\rightarrow Sn}$ distance obtained from the most extended basis sets of the two families still differ by ca. 0.06 Å.
3. The value of $E_{int}$ between the $Me_3SnCN$ molecules in the dimer amounts to −7.64 kcal/mol. This is our best estimate of $E_{int}$ obtained using the CBS(2,3) extrapolation scheme for the energies calculated at the CCSD(T)/aug-cc-pV*X*Z ($X$ = D, T) levels of theory. Both (aug)-cc-pV*X*Z and def2-*Y*ZVPP(D) basis sets produce very similar values of $E_{int}$ when the MP2 or SCS-MP2 energies are extrapolated using the CBS(3,4) scheme. In the light of the small number of theoretical investigations in which the 'def2' basis sets were employed to extrapolate energies to the CBS limit, this

insight seems to be particularly important and it proves the usefulness of the 'def2' basis sets for such purposes. Moreover, the computational cost of our calculations involving the def2-*Y*ZVPPD basis sets is lower than that required by the aug-cc-pV*X*Z basis sets with $X = Y$.

4. The $Me_3SnCN$ molecules in the dimer are held together mainly by electrostatic interactions. The SAPT calculation has shown that of all the attractive components of $E_{int}$, the electrostatic one turns out to be the largest. The occurrence of significant electrostatic forces between the $Me_3SnCN$ molecules directly affects the nature of the N → Sn coordination bond in $(Me_3SnCN)_2$. The dominant electrostatic nature of the N → Sn interaction is confirmed by the QTAIM characteristics of the bond critical point in the bond path linking the N atom and the Sn atom. The electron charge in the N → Sn region is compressed toward the N and Sn atoms and the lone electron pair of the N atom is tightly bound by this atom (as indicated also by the ELF analysis). Moreover, the N and Sn atoms involved in the N → Sn coordination develop considerable atomic charges of opposite signs when the $(Me_3SnCN)_2$ dimer is formed. The accumulation of electron charge has been detected on the N atom, whereas the electron charge depletes from the Sn atom and its NPA atomic charge reaches the value of ca. +1.65*e*. The $\Delta E^{(2)}$ energies obtained from the NBO analysis point out that the leading donor–acceptor stabilizing interaction in $(Me_3SnCN)_2$ can be assigned to the occupancy shift from the lone pair on the N atom of the coordinating $Me_3SnCN$ molecule to the σ*(Sn–CN) orbital involving the pentacoordinated Sn atom. However, the corresponding $\Delta E^{(2)}$ value suggests that it is a very weak stabilizing interaction. The direction of the CT between the $Me_3SnCN$ molecules agrees with the direction assumed by the arrow in N → Sn, but the value of the CT is very small.
5. Electrostatic interactions play the main role in the N → Sn coordination occurring in the $(Me_3SnCN)_2$ dimer and the resulting N → Sn coordination bond exhibits a predominantly ionic nature. The SAPT calculation has also revealed that the dispersion energy is required to significantly increase the energetic stabilization of the dimer. However, the resulting energetic stabilization of $(Me_3SnCN)_2$ still remains rather minor, as it is indicated by the value of $E_{int}$. The small strength of the intermolecular interaction in $(Me_3SnCN)_2$ and the important contribution of the dispersion to the energetic stabilization of the dimer make the considered N → Sn coordination similar to the formation of a weak non-bonded complex.

**Acknowledgments** This work was supported by a grant for young scientists from the University of Łódź (Grant No. 545/721). The calculations using TURBOMOLE and GAUSSIAN were carried out in the Academic Computer Center CYFRONET of the AGH University of Science and Technology in Cracow. This work was partially supported by PL-Grid Infrastructure.



## References

1. Davies AG (2004) Organotin chemistry, 2nd edn. Wiley-VCH Verlag GmbH & Co. KGaA, Weinheim
2. Evans CJ, Karpel S (1985) Organotin compounds in modern technology. Elsevier, Amsterdam
3. Champ MA, Seligman PF (1996) An introduction to organotin compounds and their use in antifouling coatings. In: Champ MA, Seligman PF (eds) Organotin environmental fate and effects. Chapman & Hall, London, pp 1–25
4. de Mora SJ (1996) The tributyltin debate: ocean transportation versus seafood harvesting. In: de Mora SJ (ed) Tributyltin: case study of an environment contaminant. Cambridge University Press, Cambridge, pp 1–20
5. Nath M (2008) The cardiovascular activity of organotin compounds. In: Gielen M, Davies A, Pannell K, Tiekink E (eds) Tin chemistry: fundamentals, frontiers, and applications. John Wiley & Sons Ltd., Chichester, pp 413–429
6. Pettinari C, Marchetti F (2008) Chemical and biotechnological developments in organotin cancer chemotherapy. In: Gielen M, Davies A, Pannell K, Tiekink E (eds) Tin chemistry: fundamentals, frontiers, and applications. John Wiley & Sons Ltd., Chichester, pp 454–468
7. Smith PJ (1998) Chemistry of tin. Blackie Academic & Professional, London
8. Mackay KM (1995) Structural aspects of compounds containing C–E (E=Ge, Sn, Pb) bonds. In: Patai S (ed) The chemistry of organic germanium, tin and lead compounds, vol 1. John Wiley & Sons Ltd., Chichester, pp 97–194
9. Baukov YI, Tandura SN (2002) Hypervalent compounds of organic germanium, tin and lead derivatives. In: Rappoport Z (ed) The chemistry of organic germanium, tin and lead compounds, vol 2. John Wiley & Sons Ltd., Chichester, pp 963–1240
10. Beattie IR, McQuillan GP (1963) Addition compounds of organotin halides with Lewis bases. J Chem Soc 1963:1519–1523
11. Hulme R (1963) The crystal and molecular structure of chloro (trimethyl)-pyridinetin(IV). J Chem Soc 1963:1524–1527
12. Avalle P, Harris RK, Hanika-Heidl H, Fischer RD (2004) Magic-angle spinning NMR spectra and re-examined crystal structure of trimethyltin cyanide. Solid State Sci 6:1069–1076
13. Lin T-P, Gualco P, Ladeira S, Amgoune A, Bourissou D, Gabbaı FP (2010) Dative P → Sn interactions in ortho-phenylene phosphine-stannanes. C R Chimie 13:1168–1172
14. Bichara LC, Fiori Bimbi MV, Gervasi CA, Alvarez PE, Brandán SA (2012) Evidences of the formation of a tin(IV) complex in citric–citrate buffer solution: a study based on voltammetric, FTIR and ab initio calculations. J Mol Struct 1008:95–101
15. Mohammadikish M (2014) Four coordinate tin complexes: synthesis, characterization, thermodynamic and theoretical calculations. Spectrochim Acta A 117:175–180

16. Koch W, Holthausen MC (2001) A chemist's guide to density functional theory, 2nd edn. Wiley-VCH Verlag GmbH, Weinheim
17. Buhl M, Kabrede H (2006) Geometries of transition-metal complexes from density-functional theory. J Chem Theory Comput 2:1282–1290
18. Jiménez-Hoyos CA, Janesko BG, Scuseria GE (2009) Evaluation of range-separated hybrid and other density functional approaches on test sets relevant for transition metal-based homogeneous catalysts. J Phys Chem A 113:11742–11749
19. Minenkov Y, Singstad Å, Occhipinti G, Jensen VR (2012) The accuracy of DFT-optimized geometries of functional transition metal compounds: a validation study of catalysts for olefin metathesis and other reactions in the homogeneous phase. Dalton Trans 41:5526–5541
20. Smith JD, Hanusa TP (2001) Trends in the structures and energetics of the group 14 metallocenes $(C_5H_5)_2M$ (M = Si-Pb): a density functional theory study. Organometallics 20:3056–3062
21. Ramırez J-Z, Vargas R, Garza J, Hay BP (2006) Performance of the effective core potentials of Ca, Hg, and Pb in complexes with ligands containing N and O donor atoms. J Chem Theory Comput 2:1510–1519
22. Broeckaert L, Turek J, Olejník R, Růžička A, Biesemans M, Geerlings P, Willem R, De Proft F (2013) Combined NMR and DFT study on the complexation behavior of Lappert's tin(II) amide. Organometallics 32:2121–2134
23. Møller C, Plesset MS (1934) Note on an approximation treatment for many-electron systems. Phys Rev 46:618–622
24. Cremer D (1998) Møller–Plesset perturbation theory. In: Clark T, Schleyer PvR, Allinger NL (eds) Encyclopedia of computational chemistry. John Wiley & Sons, Chichester, pp 1706–1735
25. Frenking G, Wagener T (1998) Transition metal chemistry. In: Clark T, Schleyer PvR, Allinger NL (eds) Encyclopedia of computational chemistry. John Wiley & Sons, Chichester, pp 3073–3084
26. Jonas V, Thiel W (1995) Theoretical study of the vibrational spectra of the transition metal carbonyls $M(CO)_6$ [M = Cr, Mo, W], $M(CO)_5$ [M = Fe, Ru, Os], and $M(CO)_4$ [M = Ni, Pd, Pt]. J Chem Phys 102:8474–8484
27. Grimme S (2003) Improved second-order Møller–Plesset perturbation theory by separate scaling of parallel- and antiparallel-spin pair correlation energies. J Chem Phys 118:9095–9102
28. Jung Y, Lochan RC, Dutoi AD, Head-Gordon M (2004) Scaled opposite-spin second order Møller–Plesset correlation energy: an economical electronic structure method. J Chem Phys 121:9793–9802
29. Lochan RC, Head-Gordon M (2007) Orbital-optimized opposite-spin scaled second-order correlation: an economical method to improve the description of open-shell molecules. J Chem Phys 126:164101
30. Szabados Á (2006) Theoretical interpretation of Grimme's spin-component-scaled second order Møller–Plesset theory. J Chem Phys 125:214105
31. DiStasio RA, Head-Gordon M (2007) Optimized spin-component scaled second-order Møller–Plesset perturbation theory for intermolecular interaction energies. Mol Phys 105:1073–1083
32. Hill JG, Platts JA (2007) Spin-component scaling methods for weak and stacking interactions. J Chem Theory Comput 3:80–85
33. King RA (2009) On the accuracy of spin-component-scaled perturbation theory (SCS-MP2) for the potential energy surface of the ethylene dimer. Mol Phys 107:789–795
34. Fink RF (2010) Spin-component-scaled Møller–Plesset (SCS-MP) perturbation theory: a generalization of the MP approach with improved properties. J Chem Phys 133:174113
35. Tkatchenko A, DiStasio RA, Head-Gordon M, Scheffler M (2009) Dispersion-corrected Møller–Plesset second-order perturbation theory. J Chem Phys 131:094106
36. Neese F, Schwabe T, Kossmann S, Schirmer B, Grimme S (2009) Assessment of orbital-optimized, spin-component scaled second-order many-body perturbation theory for thermochemistry and kinetics. J Chem Theory Comput 5:3060–3073
37. Kossmann S, Neese F (2010) Correlated ab initio spin densities for larger molecules: orbital-optimized spin-component-scaled MP2 method. J Phys Chem A 114:11768–11781
38. Goldey M, Dutoic A, Head-Gordon M (2013) Attenuated second-order Møller–Plesset perturbation theory: performance within the aug-cc-pVTZ basis. Phys Chem Chem Phys 15:15869–15875
39. Weigend F, Häser M (1997) RI-MP2: first derivatives and global consistency. Theor Chem Acc 97:331–340
40. Jung Y, Shao Y, Head-Gordon M (2007) Fast evaluation of scaled opposite spin second-order Møller–Plesset correlation energies using auxiliary basis expansions and exploiting sparsity. J Comput Chem 28:1953–1964
41. Huang Y, Shao Y, Beran GJO (2013) Accelerating MP2C dispersion corrections for dimers and molecular crystals. J Chem Phys 138:224112
42. Avalle P, Harris RK, Fischer RD (2002) DFT calculations of $^{119}$Sn chemical shifts for organometallic cyanides. Phys Chem Chem Phys 4:3558–3561
43. Pruchnik FP, Pruchnik H, Ostropolska Ł, Ciunik LZ (2008) Tris (2-cyanoethyl)tin(IV) bromide and tris(2-cyanoethyl)tin(IV) iodide, their structure, properties and reactions with adenosine, AMP and ATP. Polyhedron 27:1093–1101
44. Gholivand K, Molaei F, Rajabi M, Esrafili MD, Hosseini M (2014) Synthesis, structural characterization and DFT calculations of a new one-dimensional diorganotin(IV) derivative of *N*-isonicotinyl phosphoramide. Polyhedron 71:8–16
45. Piskunov AV, Trofimova OY, Fukin GK, Ketkov SY, Smolyaninov IV, Cherkasov VK (2012) Tin(IV) and lead(IV) complexes with a tetradentate redox-active ligand. Dalton Trans 41:10970–10979
46. Ahlrichs R, Armbruster MK, Bachorz RA, Bär M, Baron H-P, Bauernschmitt R, Bischoff FASB, Crawford N, Deglmann P, Della Sala F, Diedenhofen M, Ehrig M, Eichkorn K, Elliott S, Furche F, Glöß A, Haase F, Häser M, Hättig C, Hellweg A, Höfener S, Horn H, Huber C, Huniar U, Kattannek M, Klopper W, Köhn A, Kölmel C, Kollwitz M, May K, Nava P, Ochsenfeld C, Öhm H, Pabst M, Patzelt H, Rappoport D, Rubner O, Schäfer A, Schneider U, Sierka M, Tew DP, Treutler O, Unterreiner B, von Arnim M, Weigend F, Weis P, Weiss H, Winter N (2011) TURBOMOLE. 6.3 edn. University of Karlsruhe and Forschungszentrum Karlsruhe GmbH, 1989–2007, TURBOMOLE GmbH, since 2007, Karlsruhe
47. Neese F (2012) The ORCA program system. WIREs Comput Mol Sci 2:73–78
48. Gauss J (1998) Coupled-cluster theory. In: Schleyer PvR, Allinger NL, Clark T et al (eds) Encyclopedia of computational chemistry. John Wiley & Sons, Chichester, pp 615–636
49. Mackie ID, DiLabio GA (2011) Approximations to complete basis set-extrapolated, highly correlated non-covalent interaction energies. J Chem Phys 135:134318
50. Remya K, Suresh CH (2013) Which density functional is close to CCSD accuracy to describe geometry and interaction energy of small noncovalent dimers? A benchmark study using Gaussian 09. J Comput Chem 34:1341–1353
51. Cremer D, Kraka E, He Y (2001) Exact geometries from quantum chemical calculations. J Mol Struct 567–568:275–293
52. Raghavachari K, Pople JA (1978) Approximate 4th-order perturbation-theory of electron correlation energy. Int J Quantum Chem 14:91–100
53. Frisch MJ, Trucks GW, Schlegel HB, Scuseria GE, Robb MA, Cheeseman JR, Scalmani G, Barone V, Mennucci B, Petersson GA, Nakatsuji H, Caricato M, Li X, Hratchian HP, Izmaylov AF,

Bloino J, Zheng G, Sonnenberg JL, Hada M, Ehara M, Toyota K, Fukuda R, Hasegawa J, Ishida M, Nakajima T, Honda Y, Kitao O, Nakai H, Vreven T, Montgomery Jr. JA, Peralta JE, Ogliaro F, Bearpark M, Heyd JJ, Brothers E, Kudin KN, Staroverov VN, Keith T, Kobayashi R, Normand J, Raghavachari K, Rendell A, Burant JC, Iyengar SS, Tomasi J, Cossi M, Rega N, Millam JM, Klene M, Knox JE, Cross JB, Bakken V, Adamo C, Jaramillo J, Gomperts R, Stratmann RE, Yazyev O, Austin AJ, Cammi R, Pomelli C, Ochterski JW, Martin RL, Morokuma K, Zakrzewski VG, Voth GA, Salvador P, Dannenberg JJ, Dapprich S, Daniels AD, Farkas O, Foresman JB, Ortiz JV, Cioslowski J, Fox DJ (2013) Gaussian 09 D.01. Gaussian, Inc., Wallingford

54. HyperChem 8.0 (2007) Hypercube, Inc., Gainesville
55. Dunning TH Jr (1989) Gaussian basis sets for use in correlated molecular calculations. I. The atoms boron through neon and hydrogen. J Chem Phys 90:1007–1023
56. Peterson KA (2003) Systematically convergent basis sets with relativistic pseudopotentials. I. Correlation consistent basis sets for the post-d group 13–15 elements. J Chem Phys 119:11099–11112
57. Metz B, Stoll H, Dolg M (2000) Small-core multiconfiguration-Dirac–Hartree–Fock-adjusted pseudopotentials for post-d main group elements: application to PbH and PbO. J Chem Phys 113:2563–2569
58. Weigend F, Ahlrichs R (2005) Balanced basis sets of split valence, triple zeta valence and quadruple zeta valence quality for H to Rn: design and assessment of accuracy. Phys Chem Chem Phys 7:3297–3305
59. Rappoport D, Furche F (2010) Property-optimized Gaussian basis sets for molecular response calculations. J Chem Phys 133:134105
60. Boys SF, Bernardi F (1970) The calculation of small molecular interactions by the differences of separate total energies. Some procedures with reduced errors. Mol Phys 19:553–566
61. Halkier A, Helgaker T, Jørgensen P, Klopper W, Koch H, Olsen J, Wilson AK (1998) Basis-set convergence in correlated calculations on Ne, $N_2$, and $H_2O$. Chem Phys Lett 286:243–252
62. Halkier A, Helgaker T, Jørgensen P, Klopper W, Olsen J (1999) Basis-set convergence of the energy in molecular Hartree–Fock calculations. Chem Phys Lett 302:437–446
63. Jeziorski B, Moszyński R, Szalewicz K (1994) Perturbation theory approach to intermolecular potential energy surfaces of van der Waals complexes. Chem Rev 94:1887–1930
64. Szalewicz K, Patkowski K, Jeziorski B (2005) Intermolecular interactions via perturbation theory: from diatoms to biomolecules. Struct Bonding (Berlin, Ger) 116:43–117
65. Reed AE, Curtiss LA, Weinhold F (1988) Intermolecular interactions from a natural bond orbital, donor–acceptor viewpoint. Chem Rev 88:899–926
66. Bader RFW (1990) Atoms in molecules: a quantum theory. Clarendon, Oxford
67. Silvi B, Savin A (1994) Classification of chemical bonds based on topological analysis of electron localization functions. Nature 371:683–686
68. Bukowski R, Cencek W, Jankowski P, Jeziorska M, Jeziorski B, Kucharski SA, Lotrich VF, Misquitta AJ, Moszyński R, Patkowski K, Podeszwa R, Rob F, Rybak S, Szalewicz K, Williams HL, Wheatley RJ, Wormer PES, Żuchowski PS (2013) SAPT2012: an ab initio program for symmetry-adapted perturbation theory calculations of intermolecular interaction energies. Sequential and parallel versions. 2012.2 edn. University of Delaware and University of Warsaw, Delaware and Warsaw
69. Glendening ED, Reed AE, Carpenter JE, Weinhold F (1996) NBO 3.1. Theoretical Chemistry Institute, University of Wisconsin, Madison
70. Lu T, Chen F (2012) Multiwfn: a multifunctional wave function analyzer. J Comput Chem 33:580–592
71. Pyykkö P, Xiong X-G, Li J (2011) Aurophilic attractions between a closed-shell molecule and a gold cluster. Faraday Discuss 152:169–178
72. Kang R, Chen H, Shaik S, Yao J (2011) Assessment of theoretical methods for complexes of gold(I) and gold(III) with unsaturated aliphatic hydrocarbon: which density functional should we choose? J Chem Theory Comput 7:4002–4011
73. Grimme S, Djukic J-P (2010) The crucial role of dispersion in the cohesion of nonbridged binuclear Os → Cr and Os → W adducts. Inorg Chem 49:2911–2919
74. Papajak E, Zheng J, Xu X, Leverentz HR, Truhlar DG (2011) Perspectives on basis sets beautiful: seasonal plantings of diffuse basis functions. J Chem Theory Comput 7:3027–3034
75. Alvarez S (2013) A cartography of the van der Waals territories. Dalton Trans 42:8617–8636
76. Dvorak MA, Ford RS, Suenram RD, Lovas FJ, Leopold KR (1992) Van der Waals vs covalent bonding: microwave characterization of a structurally intermediate case. J Am Chem Soc 114:108–115
77. Papadaki H, Christofides A, Bakalbassis EG, Jeffery JC (2008) An experimental and a DFT study on the synthesis, spectroscopic characterization, and reactivity of the adducts of dimethyl- and diphenyltin(IV) dichlorides with γ-pyrones [4H-pyran-4-one (PYR) and 2,6-dimethyl-4H-pyran-4-one (DMP)]: crystal structure of $Ph_2SnCl_2$(PYR). J Organomet Chem 693:1203–1214
78. Korlyukov AA, Lyssenko KA, Baukov YI, Bylikin SY (2013) Chemical bonding in 1-(chlorodimethylstannylmethyl)-2-piperidone and its Si and Ge analogues. General trends and O → M (M = Si, Ge, Sn) coordination bond energy. J Mol Struct 1051:49–55
79. Hobza P, Müller-Dethlefs K (2010) Non-covalent interactions. Theory and experiment. RSC Publishing, Cambridge
80. Hobza P (2011) The calculation of intermolecular interaction energies. Annu Rep Prog Chem Sect C 107:148–168
81. Hobza P (2012) Calculations on noncovalent interactions and databases of benchmark interaction energies. Acc Chem Res 45:663–672
82. Neese F, Valeev EF (2011) Revisiting the atomic natural orbital approach for basis sets: robust systematic basis sets for explicitly correlated and conventional correlated ab initio methods? J Chem Theory Comput 7:33–43
83. Gurvich LV, Veyts IV, Alcock CB (1994) Thermodynamic properties of individual substances, vol 3, 4th edn. Hemisphere Publishing Corporation, New York
84. Smith EL, Sadowsky D, Phillips JA, Cramer CJ, Giesen DJ (2010) A short yet very weak dative bond: structure, bonding, and energetic properties of $N_2$–$BH_3$. J Phys Chem A 114:2628–2636
85. http://www.physics.udel.edu/~szalewic/SAPT/SAPT.html. Accessed 1 May 2014
86. Patkowski K, Szalewicz K (2007) Frozen core and effective core potentials in symmetry-adapted perturbation theory. J Chem Phys 127:164103
87. Zahn S, Uhlig F, Thar J, Spickermann C, Kirchner B (2008) Intermolecular forces in an ionic liquid ([Mmim][Cl]) versus those in a typical salt (NaCl). Angew Chem Int Ed 47:3639–3641
88. Karthikeyan S, Sedlak R, Hobza P (2011) On the nature of stabilization in weak, medium, and strong charge-transfer complexes: CCSD(T)/CBS and SAPT calculations. J Phys Chem A 115:9422–9428
89. Girichev GV, Giricheva NI, Koifman OI, Minenkov YV, Pogonin AE, Semeikind AS, Shlykov SA (2012) Molecular structure and bonding in octamethylporphyrin tin(II), $SnN_4C_{28}H_{28}$. Dalton Trans 41:7550–7558
90. Nechaev MS, Ustynyuk YA (2005) Molecular geometry and electronic structures of stable organic derivatives of divalent germanium and tin $[(Me_3Si)_2N–M–OCH_2CH_2NMe_2]_n$ (M = Ge,

n = 1; M = Sn, n = 2): a theoretical study. Russ Chem Bull Int Ed 54:108–116
91. Martin F, Zipse H (2005) Charge distribution in the water molecule—a comparison of methods. J Comput Chem 26:97–105
92. Bader RFW (1998) A bond path: a universal indicator of bonded interactions. J Phys Chem A 102:7314–7323
93. Espinosa E, Alkorta I, Elguero J, Molins E (2002) From weak to strong interactions: a comprehensive analysis of the topological and energetic properties of the electron density distribution involving X–H···F–Y systems. J Chem Phys 117:5529–5542
94. Jonas V, Frenking G, Reetz MT (1994) Comparative theoretical study of Lewis acid-base complexes of $BH_3$, $BF_3$, $BCl_3$, $AlCl_3$, and $SO_2$. J Am Chem Soc 116:8141–8753
95. Karlov SS, Tyurin DA, Zabalov MV, Churakov AV, Zaitseva GS (2005) Quantum chemical study of group 14 elements pentacoordinated derivatives—metallatranes. J Mol Struct 724:31–37
96. Bates PA, Hursthouse MB, Davies AG, Slater SD (1989) The structure of 2,2-di-t-butyl-1,3,2-dioxa-, -oxathia-, and -dithiastannolanes: a study by solution and solid state NMR and single crystal X-ray diffraction. J Organomet Chem 363:45–60